Materials Chemistry and Physics 242 (2020) 122449

Contents lists available at ScienceDirect

Materials Chemistry and Physics

journal homepage: www.elsevier.com/locate/matchemphys

Microwave assisted synthesis of $CuInGaSe_2$ quantum dots and spray deposition of their composites with graphene oxide derivatives

Kalenga Pierre Mubiayi [a,b], Diogo Martinez Guilhermitti Neto [c], Andreia Morais [c], Helton Pereira Nogueira [c], Thebano Emílio de Almeida Santos [c], Talita Mazon [c], Nosipho Moloto [a], Makwena Justice Moloto [b], Jilian Nei Freitas [c,*]

[a] Molecular Science Institute, School of Chemistry, University of the Witwatersrand, P. Bag 03, Wits, 2050, South Africa
[b] Department of Chemistry, Faculty of Applied and Computer Science, Vaal University of Technology, P. Bag X021, Vanderbijlpark, 1900, South Africa
[c] Center for Information Technology Renato Archer – CTI, Rodovia D. Pedro I, Km 143,6, 13069-901, Campinas, SP, Brazil

HIGHLIGHTS

- Microwave assisted synthesis of tetragonal phase crystalline $CuInGaSe_2$ quantum dots.
- $CuInGaSe_2$ composites with GO or rGO were processed from aqueous solutions.
- Thin, homogeneous films prepared with an automated ultrasonic spray system.
- Morphological, optical and electrical properties were investigated.
- The films were used as a counter electrode in dye-sensitized solar cells.

GRAPHICAL ABSTRACT

ARTICLE INFO

Keywords:
Copper indium gallium selenide
Microwave assisted synthesis
Spray deposition
Graphene oxide
Reduced graphene oxide
Dye-sensitized solar cell

ABSTRACT

In this contribution, we explore a spray deposition technique to prepare thin films based on nanocomposites of graphene oxide (GO) or reduced graphene oxide (rGO) with $CuInGaSe_2$ quantum dots (QD) synthesized by a microwave-assisted method. Small nanocrystals in the tetragonal phase and emitting light at 650 nm were obtained. Water-based solutions of the nanocomposites were sprayed onto transparent conductive glass substrates using an automated ultrasonic spray system and the resulting thin films were evaluated with respect to their morphological and electrochemical properties. The distribution and organization of the graphene sheets in the composites were affected by the interaction between the nanocrystals and GO or rGO, which also interfered on the electronic properties. In addition, we demonstrated a possible application of the thin film based on the rGO-QD composite as a counter electrode in dye-sensitized solar cells.

1. Introduction

Copper indium gallium selenide (CIGSe) materials are I-III-VI p-type semiconductors that possess high optical absorption coefficients and low band gap energy. Because of these features, bulk CIGSe has been successfully applied in thin film solar cells with ca. 20% of efficiency [1,2]. Lately, there has been a growing interest in the synthesis of nano-sized CIGSe and other quaternary quantum dots (QDs), aiming at further improving the efficiency of the solar cells and the reduction of costs by using lower amounts of materials.

The synthesis of CIGSe can be performed using vacuum or non-vacuum techniques. Significant energy input is typically required in

* Corresponding author.
E-mail address: jilian.freitas@cti.gov.br (J.N. Freitas).

https://doi.org/10.1016/j.matchemphys.2019.122449
Received 1 August 2018; Received in revised form 4 November 2019; Accepted 13 November 2019
Available online 14 November 2019

vacuum techniques, such as evaporation or sputtering. Therefore, alternative, non-vacuum, solution-based techniques have drawn crescent interest. Examples of non-vacuum tecnhniques used to synthesize CIGS from chemical precursors include refluxing [3], solvothermal [4], precipitative [5] and colloidal [6] methods, as well as the microwave assisted method [7–9]. In these solution-based techniques, organic solvents and high temperatures are often used. The reaction time, temperature, solvent and other preparation conditions are key parameters to minimize the size distribution of the CIGSe nanoparticles and the formation of undesired by-products.

Amongst the different non-vacuum techniques, the microwave assisted method generally offers advantage regarding a record reaction time, combined with relatively low temperatures, at low energy consumption. Microwave energy is considered as a heat source that leads to faster chemical reactions in comparison to conventional heating methods. The reaction rate is affected by the microwave field and the quality of the generated material depends on the type of reactant, applied power, reaction time and temperature [8]. The use of microwave heating for the preparation of CIGSe nanopowder has been previously reported [7,8].

Solution processing techniques are also appealing because of their potential low cost and high yield, and possibility of incorporation in a roll-to-roll (R2R) line. One example of solution processing deposition method is the spray coating technique. This deposition technique has numerous applications in industry, like in the painting, coating and graphic industry. There has also been a grown interest in the use of spray deposition for other fields, such as electronics and photovoltaics [10–14]. Recently, Kramer et al. [10] simulated a R2R processing line for the spray deposition of PbS QDs. The films were sprayed onto substrates mounted on a rapidly rotating drum and then successfully used as the active layer of solar cells with a depleted heterojunction architecture. Furthermore, the use of ultrasonic spray nozzles might allow the deposition of uniform films and improve reproducibility over larger areas [11,12].

Herein, we report the synthesis of $CuInGaSe_2$ QDs using a microwave assisted method, and the solution processing via spray deposition of thin films based on the combination of these QDs with graphene oxide (GO) or reduced graphene oxide (rGO). Because of the electronic and optical characteristics of these materials, nanocomposites based on the combination of GO and rGO with quantum dots can be used in a variety of applications, ranging from biomedical optical imaging [15], to light-controlled conductive switching [16] and photocatalytic CO_2 reduction [17], for example. In this work, we demonstrate the possibility of exploring such films for energy conversion by using the rGO-QD thin film as a counter electrode in dye-sensitized solar cells (DSSCs). DSSCs have drawn a lot of attention because of their easy fabrication process. A lab-scale DSSC may be assembled in a bench top, from solution-processed materials, without the need of expensive machinery or techniques [18]. A typical DSSC consists of a dye-sensitized TiO_2 photoanode, a liquid electrolyte (typically containing the I^-/I_3^- redox couple) and a Pt counter electrode. Amongst these components, there is interest in finding a replacement for Pt, due to the high costs associated with this noble metal. Graphene-based materials have been explored as alternatives, because these materials possess high electrical conductivity and chemical and mechanical robustness [19]. Their composites with cupper chalcogenide-based quantum dots have also been strategically used as counter electrodes and are particularly advantageous when combined with electrolytes containing different redox couples, in substitution to the corrosive I^-/I_3^- [20,21].

2. Experimental details

2.1. Materials

Copper (I) chloride (CuCl), indium chloride ($InCl_3$), gallium chloride ($GaCl_3$), selenium powder, tri-n-octylphosphine (TOP), oleylamine (OLA), mercapto-propionic acid (MPA), ethane dithiol (EDT), TiO_2 (DSL 18NR-T, Dyesol), N749 (Dyesol), expansible graphite (Grafexp, Nacional de Grafite), hydrazine, acetonitrile, hexane, methanol, ethanol and acetone were used as received.

2.2. Synthesis of CIGSe QD using microwave assisted method (MAM)

In a typical synthesis, 2 ml of 1 M TOPCuCl, 0.5 ml of 1.0 M $TOPInCl_3$ and 0.5 ml of 1.0 M $TOPGaCl_3$ were added to 5 ml of OLA in a Teflon vessel liner, mounted on the rotor, and then purged with argon for 2 min before being placed in the microwave. The microwave was then heated for 10 min at a power of 500 W. The system was then cooled to 70 °C and 1 ml of 2 M TOPSe was quickly added. The vessel was then purged for 5 min with argon before continuing heating the mixture for another 10 min at 600 W. The heating was stopped and the vessels were allowed to cool to 50 °C. Methanol was then added to the solution to flocculate the nanoparticles and CIGSe QDs were collected after centrifugation.

2.3. Ligand exchange

Ligand exchange was performed by adding 10 mL of an aqueous solution (pH 10 adjusted with tetrabutylammonium hidroxide) containing 1.6 mmol of MPA to 30 mg of the QDs powder and keeping under stirring at 50 °C for 72 h. The resulting nanoparticles were precipitated with acetone and isolated after centrifugation, then dispersed in isopropanol at the concentration of 6 mg/mL.

2.4. Preparation of GO and rGO

Graphitic oxide was prepared according to a modified Hummer's method [22]. Pre-oxidizing reaction was carried out by adding 10 g of expansible graphite into an Erlenmeyer flask containing 30 mL of concentrated sulfuric acid, 5 g of potassium persulfate and 5 g of phosphorus pentoxide at 80 °C. After 6 h of reaction, the solid was washed until neutralization. The pre-oxidized graphite was submitted to a new oxidizing process in an Erlenmeyer flask containing 460 mL of concentrated sulfuric acid, 5 g of sodium nitrate and 30 g potassium permanganate. After 2 h, deionized water was added and the mixture was heated to 100 °C for 15 min. The reaction was quenched by the addition of 50 mL of hydrogen peroxide 30 vol%. The solid was washed until the complete removal of manganese ions and then dispersed in deionized water and submitted to dialysis process for about three weeks to remove residual ions. The aqueous suspension of graphite oxide was submitted to sonication, to afford the GO sample.

The GO aqueous suspension was submitted to ultrasonication for 1h and then reduced with hydrazine (1% vol) under constant stirring at 60 °C for 6h, to afford the rGO aqueous suspension.

2.5. Preparation of the composites

Nanocomposites were obtained by sonicating for 1h a mixture containing 1.5 mL of the $CuInGaSe_2$ QD solution (concentration 6 mg/mL) and 100 mL of the GO or rGO aqueous suspension (concentration 0.12 mg/mL).

2.6. Thin film deposition

Before spraying, the dispersions were homogenized for 30 min in an ultrasonic bath. Ultrasonic spray depositions were performed using an ExactaCoat coating system (Sonotek Corp., Milton, USA) with an AccuMist™ nozzle. The injection flow rate was adjusted to 0.125 mL/min and 50 layers were sprayed onto TCO substrates. The heating plate of the equipment was kept at 100 °C during the deposition.

2.7. Characterization of CIGSe QDs and thin films

The synthesized CIGSe QDs were dispersed in toluene and placed in a quartz cuvette for optical measurements. A Perkin Elmer LS45 fluorescence spectrophotometer was used to analyze the photoluminescence (PL) of the as-synthesized nanocrystals. The absorbance measurements were determined using an Analytica Jena Specord 5D UV–vis Spectrophotometer. Transmission electron microscopy (TEM) images of samples drop cast from the toluene dispersion were obtained with a FEI G^2 Tecnai spirit transmission electron microscope. The structural properties were determined using Bruker D2 Phaser X-ray diffractometer on crushed samples. Scanning electron microscopy (SEM) images of the sprayed thin films were obtained with a FEI Inspect F50 microscope. Energy dispersive X-ray spectrometry (EDS) analysis were carried out in a Tescan Mira 3 FEG-SEM microscope. Optical microscopy images of the thin films were taken with an Olympus B51x microscope (Olympus Corp., USA). Atomic force microscopy (AFM) images were acquired with a Nanosurf, EasyScan2 microscope, operating in the tapping mode. Raman spectra of the films were recorded in a Raman confocal spectrometer (Horiba Jobin Yvon model T64000) with 514 nm excitation wavelength and the transmittance was measured with a Perkin Elmer Lambda 900 UV/VIS/NIR spectrophotometer. Cyclic voltammetry was performed in a three electrode electrochemical cell using the sprayed films as working electrode, a Pt wire as counter electrode and Ag/AgCl as reference, in a 0.05 M phosphate-buffered saline (PBS) electrolyte. The electrochemical properties of the thin-films in the presence of a liquid electrolyte containing either the thiolate/disulfide redox couple (prepared according to the literature [23]) or the I^-/I_3^- redox couple (EL-HSE, Dyesol) were investigated using a symmetric cell, where the electrolyte was sandwiched between two electrodes made from films of the same type. The space between the electrodes (~100 μm) and active area (1 cm^2) were controlled with an adhesive tape. Electrochemical impedance spectroscopy (EIS) measurements were performed using an Autolab PGSTAT302 N potentiostat with a FRA module, in the frequency range of 0.1–10^6 Hz, with amplitudes of ±10 mV over the open circuit potential. The experimental data were fitted using the Boukamp software. Surface resistivity was measured by four-point probe technique (Thin Film Devices, INC, model FPP-2000).

2.8. Solar cell assembly and characterization

A sandwich-type DSSC was assembled with 0.25 cm^2 of active area. The TiO_2 nanoporous film was prepared by doctor blading a small aliquot of a commercial colloidal suspension onto a TCO substrate (TCO 22-7, Solaronix) and heating to 450 °C for 30 min. This electrode was then immersed in a 0.15 mmol L^{-1} ethanolic solution of the N719 sensitizer for 20 h at room temperature and, afterwards, washed with ethanol and dried in air. A thin plastic film was used as spacer (60 μm) between the photoelectrode and the counter electrode (Pt or the rGO-QD film), and the cell was filled with a liquid electrolyte. The electrolyte consisted either of a commercially available electrolyte containing the I^-/I_3^- redox couple (EL-HSE, Dyesol), or an electrolyte containing the thiolate/disulfide (T^-/T_2) redox couple, prepared according to the literature [23]. The current−voltage ($J-V$) curves of cells exposed to irradiation of a solar simulator SS-0.5K (Sciencetech) adjusted to 100 mW cm^{-2} were measured with a 2410C Keithley source meter. The open circuit voltage (*Voc*), short-circuit current density (*Jsc*), fill factor (*FF*), and power conversion efficiency (*PCE*) parameters were extracted from the $J-V$ curves.

3. Results and discussion

3.1. Synthesis of CIGSe QDs

The optical properties of as-synthesized CIGSe are shown in Fig. 1a. A large tailing of the UV–Vis absorption curve was observed. This profile is similar to that reported in previous studies using microwave-assisted synthesis of CIGSe [7] or other solution-based synthetic routes [24]. A broadening of the absorption spectrum and band tail effects may be related to the presence of intrinsic defects, since the breadth of the absorption tail is a strong function of the disorder. The absorption band edge was found at *ca.* 550 nm. The large blue-shift of the absorption wavelength in relation to the characteristics of bulk CIGSe crystals indicates that the CIGSe QDs prepared here have dimensions in the quantum confinement region. Fig. 1b displays a plot calculated from the absorption curve using the Tauc model [25]. The band gap of the CIGSe nanoparticles estimated from this plot corresponds to ~2.0 eV, which is larger than the typical band gap found for bulk CIGSe (1.04–1.67 eV [26]). Quantum confinement effects and structural defects in cooper selenides might lead to the blue shift of the band gap [27]. Increased band gaps have also been related to poor crystallinity. Furthermore, the presence of secondary phases, as well as the coordination bonding of the capping ligand also affect the optical features [28]. An emission band centred at 650 nm with a FWHM of 38 nm was observed in the PL spectra (Fig. 1a), indicative of a large polydispersivity of the sample.

TEM analysis was performed to confirm the structure of synthesized CIGSe QDs. As shown in Fig. 1c, pyramidal shapes were the most dominant (A), but were being transformed into bipyramidal (B) or other shapes (C) upon growth. Nevertheless, the crystals were small, with sizes up to *ca.* 10 nm. The existence of different shapes and broad size distribution in non-uniform samples could be related to a non-uniform heating from the microwave energy source used. Heating uniformity is a key factor in microwave-assisted syntheses. On the other hand, other authors reported CIGSe samples with even larger particles and broader size distributions using microwave synthesis [8] or other methods [24]. Fig. 1d shows the crystallinity of the synthesized CIGSe QDs. A tetragonal phase of $CuIn_{0.5}Ga_{0.5}Se_2$ was attributed to the sample with the presence of all major peaks (JCPDS #40-1488).

3.2. Solution processing and thin film deposition

Nanocomposites were used in this work to suppress challenges associated with the use of low quantities of QDs and the low conductivity of the QDs capped with bulky ligands. GO and rGO were selected as components for the composites due to the favorable interaction between these materials and several chalcogenide-based QDs, as demonstrated in previous reports [29–31]. Defects and surface edges in graphene can act as catalysts and the surface modification by introduction of heteroatoms further increases the number of active sites, whereas also serving as effective anchoring sites for inorganic nanoparticles. Thus, in such composites, the GO and rGO act as a matrix where the QDs are dispersed. Furthermore, in the particular case of rGO, the conductivity of the composite film might be enhanced because of the electronic nature of this material.

As-synthesized CIGSe QDs were capped with OLA. This capping ligand was selected based on previous results, where it was found that the use of OLA in a conventional colloidal method of synthesis allowed the formation of well dispersed and relatively small sized $CuIn_{0.75}Ga_{0.25}Se_2$ nanoparticles [32]. OLA acts as both the reaction solvent and surfactant, and has been shown to passivate the nuclei and slow down the growth rate of the particles, by reducing the relative reactivity between the precursors, which is crucial for the control of the stoichiometry [33], as well as for the control over the particle size [8,32].

Here, aiming at the combination of the CIGSe QDs with GO and rGO, after the synthesis of the QDs, a post-production ligand exchange reaction was performed using MPA. The MPA-capped QDs present higher solubility in polar solvents and, therefore, are more suitable for mixing with the aqueous GO and rGO suspensions. The GO-QD and rGO-QD nanocomposites were obtained by mixing the materials in an ultrasonic bath for 1 h. Fig. 2 shows pictures of the aqueous dispersions used for spray coating, the automated equipment used for deposition, and the resulting thin films. Films based solely on GO and rGO were also

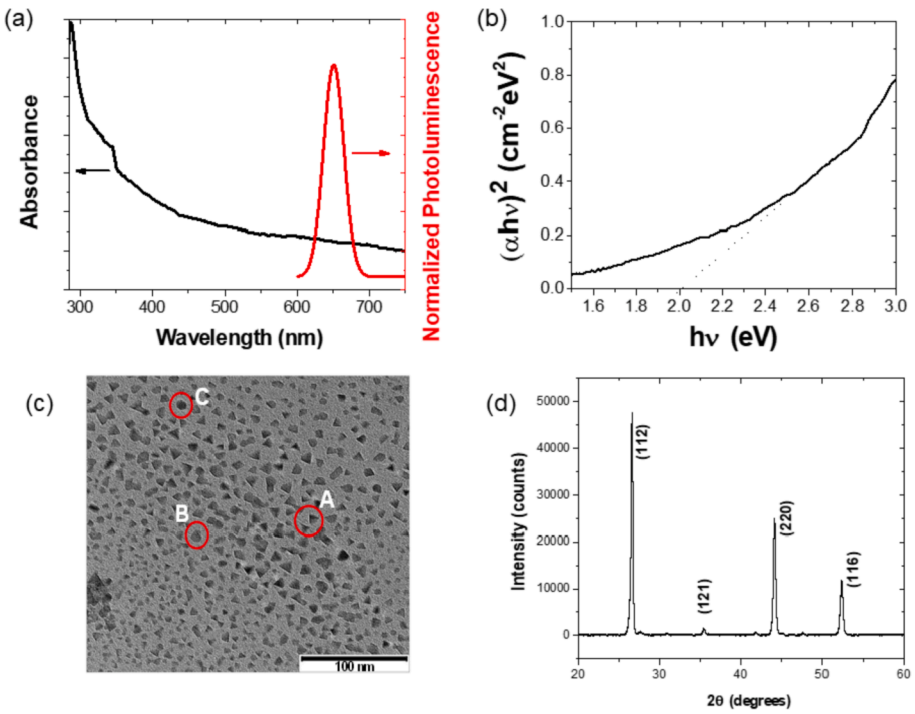

Fig. 1. (a) UV–Vis absorption spectra and PL emission spectra of as-synthesized CISe QDs and (b) Tauc plot from the absorption curve. (c) TEM image of CIGSe QDs, where (A), (B) and (C) represent the mixture of shapes found in the sample. The scale bar indicates 100 nm. (d) X-Ray diffraction pattern of as-synthesized CIGSe QDs with indices matching tetragonal phase of $CuIn_{0.5}Ga_{0.5}Se_2$ (JCPDS #40-1488).

prepared, for comparison.

The deposition of smooth, homogeneous films from dispersions containing materials like GO, rGO and QDs may be challenging, because they may form large particle aggregates or precipitate. These effects are even more likely to happen during a slow deposition method, like spraying, where several layers must be deposited to allow the formation of films with appreciable thicknesses. The investigation of the morphological characteristics of the films is extremely important, because the optical and electronic properties of QDs, and GO or rGO are strongly related to the structure of the film [34,35], which is, in turn, affected by the preparation method. Figs. 3 and 4 display images acquired with optical microscopy and AFM, respectively, for as-deposited thin films of GO, rGO, GO-QD or rGO-QD. From the images, it is possible to see that the morphology of the films change significantly after the incorporation of QDs, where the larger sheets, rolled up sheets and domains existing in the neat GO and rGO films seem to be disrupted by the interaction with the inorganic nanoparticles in the GO-QD and rGO-QD composites. On the other hand, a larger number of small clusters appear

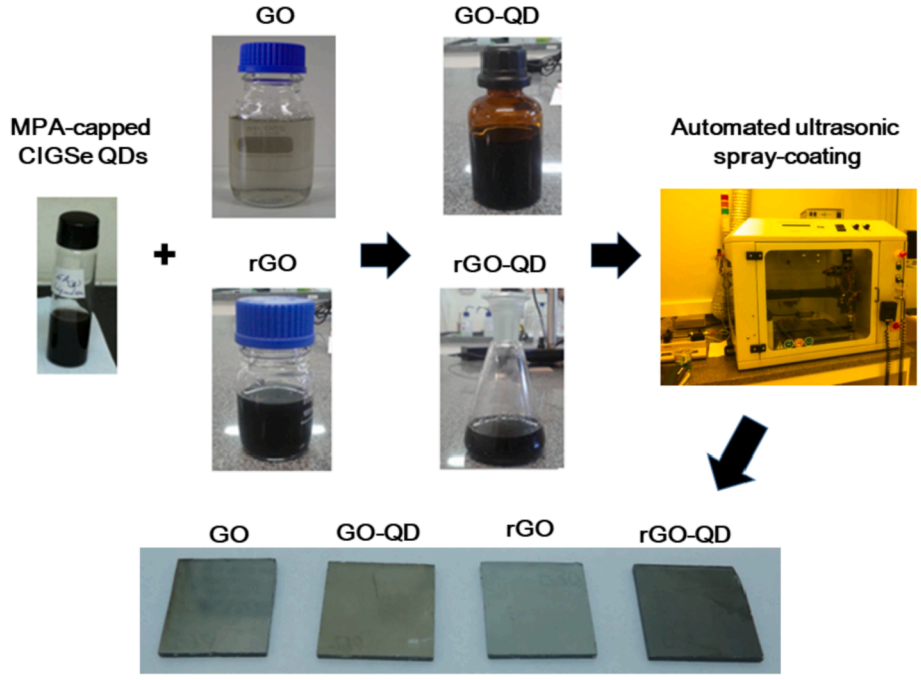

Fig. 2. Pictures of the QDs, GO, rGO, GO-QD and rGO-QD dispersions used for spray coating, the automated spray equipment, and the resulting thin films.

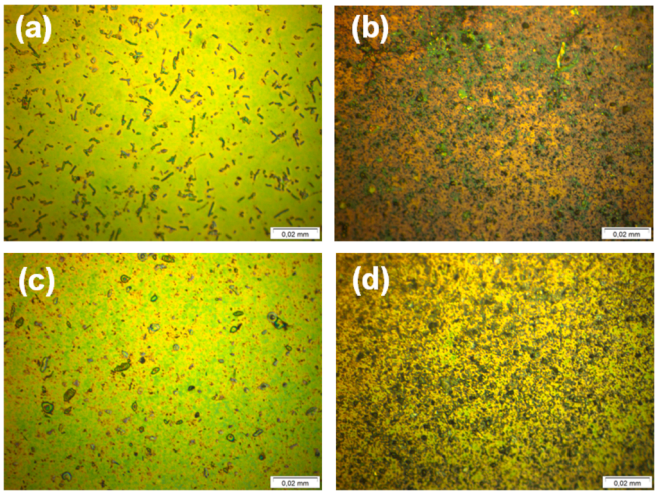

Fig. 3. Optical microscopy images of films containing (a) GO, (b) GO-QD, (c) rGO and (d) rGO-QD. The scale bar indicates 0.02 mm in all images (magnification = 50X).

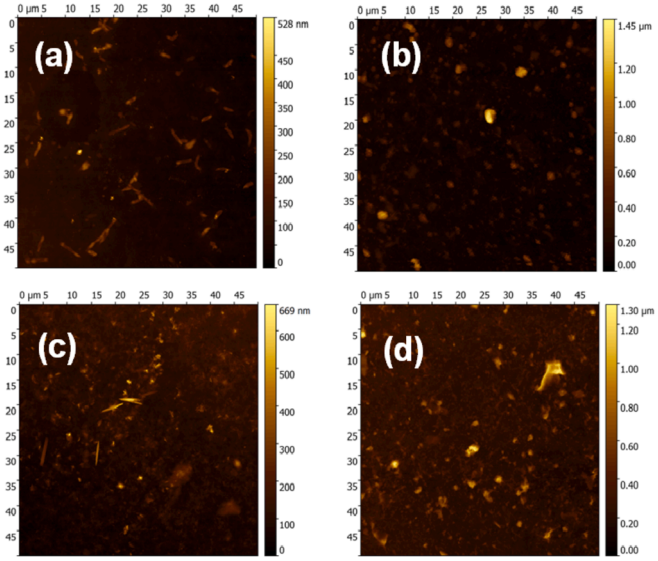

Fig. 4. AFM images in the tapping mode for films containing (a) GO, (b) GO-QD, (c) rGO and (d) rGO-QD. The scanning area was 50 μm × 50 μm in all images.

in these composites. The root mean square (RMS) roughness estimated from the AFM images in Fig. 4 is approximately 35 nm and 54 nm for GO and rGO, and is enhanced to 104 nm and 113 nm for the GO-QD and rGO-QD films, respectively.

The differences in the morphology are also evident in the SEM images of the films, displayed in Fig. 5. The GO-QD and rGO-QD films show rougher surfaces with a higher density of agglomerates, where it is noted the formation of regions containing clusters with more spherical shape and dimensions around 30–80 nm, as exemplified in the regions highlighted with red circles in Fig. 3b,d. The presence of QDs in the films was confirmed by EDS analysis, where the elements Cu, In Ga and Se, and S from the MPA ligands, were found. Other elements, such as C and O, from the graphene layers, and Sn, O, F, Si and Na from the TCO substrate were also observed. The substrate pattern can be seen in all images of Fig. 5. Unfortunately, it was not possible to estimate unequivocally the thickness of the films with any of the available techniques.

The differences observed in the morphology of the neat GO and rGO films in comparison with the GO-QD and rGO-QD films are indicative

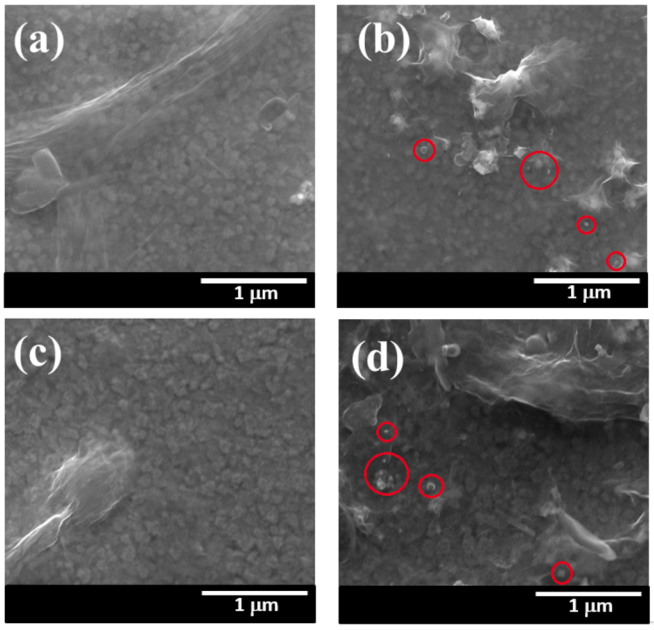

Fig. 5. FEG-SEM images of the films containing (a) GO, (b) GO-QD, (c) rGO and (d) rGO-QD. The scale bar indicates 1 μm in all images and the red circles indicate regions with the presence of large clusters of QDs.

that the interaction of these materials with the QDs introduced more defects in the nanocomposite films.

The films were further investigated with Raman spectroscopy. Fig. 6 displays the typical graphene response, where the G band (vibration of sp^2 carbon atoms) and the D band (disordered sp^3 carbons on graphene surface) are observed in all samples. The corresponding data are listed in Table 1.

The chemical reduction of GO to rGO resulted in an increase of the I_D/I_G ratio (intensity of the bands D and G), attributed to the formation of unrepaired defects after the removal of oxygen functionalities, which is considered indicative of effective reduction of GO [36,37]. A clear enhancement of the I_D/I_G ratio is also observed for the GO-QD and rGO-QD nanocomposites in comparison to the films containing the neat GO or rGO. This indicates that a significant number of structural defects were introduced in the composite films, possibly related to a bending or breaking of the graphene sheets after the physical interaction with the inorganic nanoparticles. A similar enhancement of the I_D/I_G ratio has been reported for nanocomposites of rGO and CdS QDs [29]. This

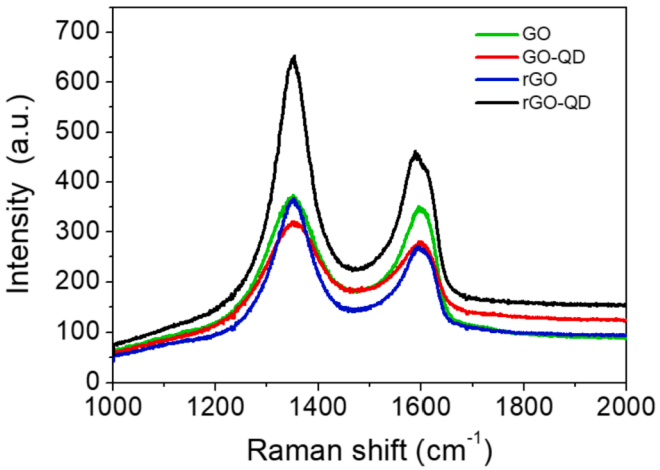

Fig. 6. Raman spectra of thin films of (—) GO, (—) GO-QD, (—) rGO and (—) rGO-QD.

Table 1
Data extracted from the Raman spectra.

Thin film	D-band (cm^{-1})	G-band (cm^{-1})	I_D/I_G ratio
GO	1352.09	1596.02	1.06
rGO	1350.44	1597.68	1.14
GO-QD	1349.33	1597.68	1.36
rGO-QD	1347.68	1590.51	1.41

enhanced manifestation of defects in the composites is in agreement with the findings from the microscopy images of the films, as previously discussed.

A significant change in the optical transparency of the thin films was also observed, with a strong decrease of transmittance in the visible range for GO-QD and rGO-QD films, in comparison to the GO or rGO films (Fig. 7), related to the presence of CIGSe QDs in the nanocomposites. Nevertheless, all films retain some degree of transparency in the visible region. This feature is interesting for several applications. For example, the use of semitransparent counter electrodes in solar cells is considered an advantage for building integration photovoltaics and for the development of bi-facial solar panels.

Fig. 8 displays the cyclic voltammograms of the sprayed films measured in a three-electrode configuration, with Ag/AgCl as reference. The bare TCO substrate does not shows any appreciable response in the electrochemical region investigated here. For the GO thin film, the reduction process was more evident than the oxidation process. The reduction peak, centred at ~ −0.7 V, is attributed to the electrochemical reduction of oxygen-containing groups in GO prepared by the oxidation using permanganate oxidants [38]. The peak at ~ -0.7 V can also be seen in the voltammogram of the GO-QD film, but it is not as evident in the voltammograms of rGO and rGO-QD. This is attributed to a deoxygenation upon the reduction process during the preparation of rGO from GO. Simultaneously, it was observed that the onset of the reduction process is shifted towards less negative bias for rGO and for the composite samples, in comparison to the GO film: the onset of the reduction process is observed at −0.278 V, −0.219 V, −0.150 V and −0.135 V for GO, GO-QD, rGO and rGO-QD films, respectively. This change is related to a change in the electron affinity of the carbonaceous material, with a shift of the energy of the LUMO level [39]. The electroctrochemical behavior of permanganate-oxidized GO samples, such as the materials investigated here, has been studied in previous reports and it was found that there is a complex relation between their response and redox cycling [38]. A detailed investigation into the mechanisms and electrochemical behavior of these systems is beyond the scope of the present study.

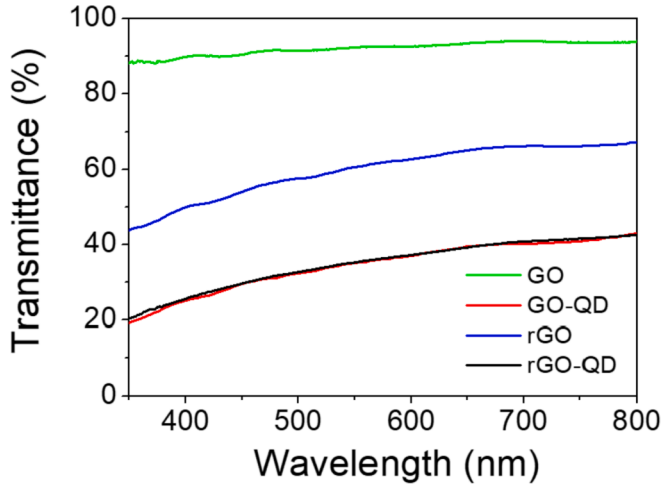

Fig. 7. Transmittance of thin films of (▬) GO, (▬) GO-QD, (▬) rGO and (▬) rGO-QD.

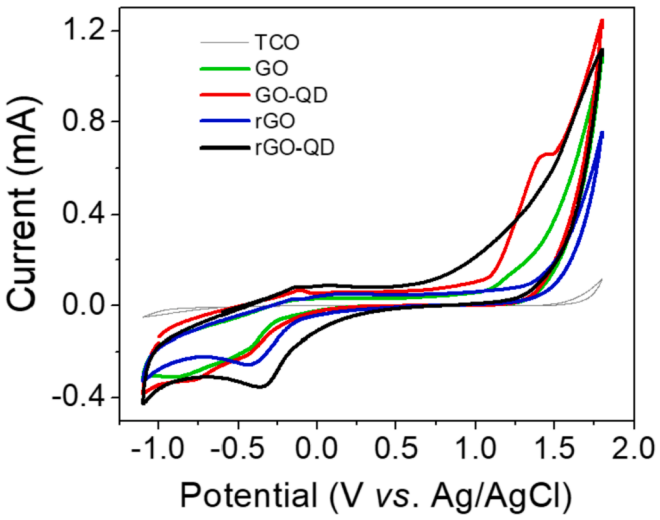

Fig. 8. Cyclic voltammetry analysis of (–) the bare TCO substrate and films of (▬) GO, (▬) GO-QD, (▬) rGO and (▬) rGO-QD (scan rate = 20 mV s^{-1}).

Ex situ methods for the assembly of nanoparticles on the surface of graphene or its derivatives, in which the nanoparticles are presynthesized separately and then attached to graphene, like the method investigated here, are frequently explored. In this method, the attachment of the nanoparticles can be achieved by means of a chemical bonding (using linking agents, such as molecules containing thiol or amine groups) or via non-covalent interactions, such as van der Waals, π–π stacking, or electrostatic interactions. The loading of nanoparticles to GO may be higher in comparison to rGO, due to the larger amount of oxygen-containing groups on the GO surface. Although *ex situ* methods usually offer the advantage of providing good control over the size, shape and functionality of the nanoparticles, it can also lead to weaker interactions between the inorganic particles and the carbonaceous material in comparison to the cases where the particles are directly synthesized in the presence of graphene species (*in situ* methods). A study of composites of rGO-CdTe using cyclic voltammetry has demonstrated how the electrochemical properties are more affected when the composites are prepared by *in situ* method, rather than by a physical mixture of rGO and CdTe (*ex situ* method) [40]. Regardless, in either case, the physical and chemical properties of the surfaces and interfaces involved in graphene-nanoparticle composites is of utmost importance. The interfacial structure, interaction, and interface impurities lead to changes in the morphology and electronic structure of graphene, whereas the bandgap of semiconductors can also be affected by their bonding with graphene. For detailed discussions regarding the role of surfaces and interactions between graphene and inorganic semiconductors, the reader is directed to excellent reviews available in the literature [41,42].

In spite of the fact that an *ex situ* method was used in this study, the changes observed in microscopy images, Raman spectra and cyclic voltammograms of the films containing the composites with QDs, in comparison to the neat GO or rGO films, attest that there is a significant interaction between the materials in the composites investigated here. Although we cannot specify the exact type of interaction that occur in these composites, it is possible to state that it is strong enough to change the distribution/organization of the graphene sheets and their energy levels.

3.3. Application in solar cells

A possible application for the films prepared here is their use as counter electrodes in DSSCs. Reports using only rGO [43–45], or CIGSe films prepared by magnetron sputtering [46] or a nebulizer spray

pyrolysis technique at 350 °C [47], as counter electrodes for DSSCs, achieved *PCE* values varying from 1.7 to 7.62%, revealing the suitability of these materials for this kind of application.

The main function of the counter electrode in a DSSC is to provide the pathway for electron transfer from the external circuit to the electrolyte, catalyzing the reduction of the oxidized species. As proof of concept, DSSCs were assembled using the rGO-QD film as counter electrode, in the presence of two different electrolytes. Fig. 9 exhibits the *J-V* curves obtained for the cells under irradiation of a solar simulator (AM 1.5 conditions, intensity of 100 mW cm^{-2}) and the parameters extracted from the *J-V* curves are displayed in Table 2.

The DSSC assembled with rGO-QD counter electrode and the I^-/I_3^--based electrolyte delivered a *Jsc* of 8.78 mA cm^{-2}, *Voc* of 0.69 V and *FF* of 33%, resulting in a *PCE* of 2.00%. The cell assembled with the less corrosive T^-/T_2 electrolyte delivered a *Jsc* of 7.16 mA cm^{-2}, *Voc* of 0.45 V and *FF* of 35%, resulting in a *PCE* of 1.14%. These results suggest that the main limitation of the DSSCs assembled with the rGO-QD film as counter electrode is related to a low *FF* value. Regardless of the electrolyte composition, the cells presented similar FF values (33%–35%). From four-point probe measurements, the surface resistivity of the sprayed films was estimated to be 8.22 Ω/sq, 8.12 Ω/sq, 8.15 Ω/sq and 8.03 Ω/sq for the GO, GO-QD, rGO and rGO-QD film, respectively, which is close to the resistivity measured for the neat TCO substrate (8.48 Ω/sq). This, in turn, introduced a high series resistance (R_s) in the device, which is one of the factors associated with low *FF* values.

To further investigate the electrochemical behavior of these counter electrodes, EIS analysis was carried out in symmetric cells prepared by stacking two electrodes of rGO-QD facing each other, separated by a 100 μm spacer and filled with a liquid electrolyte containing either the I^-/I_3^- or the T^-/T_2 redox couple. The Nyquist and Bode plots are shown in Fig. 10. The inset illustrates the R(RQ) circuit used to fit the experimental data, where R_s is the ohmic serial resistance, R_{ct} is the charge-transfer resistance and CPE is the constant phase angle element at the electrolyte/counter electrode interface. The parameters extracted from the EIS measurements are summarized in Table 2. The R_s values originated from the poor conductivities of these films, as discussed above. Furthermore, the large R_{ct} values (~1.2–1.6 kΩ) suggest that the efficiency of the rGO-QD films towards the electron transfer kinetics for electrolyte regeneration has to be improved. The larger CPE observed for the cell assembled with the I^-/I_3^- electrolyte may be associated with charge accumulation/trapping at the interface electrode/electrolyte. This is in agreement with the "S-shaped" profile of the *J-V* curve observed for this cell (displayed in Fig. 9). This behavior has been previously reported for DSSCs assembled with a spray-coated rGO counter electrode and was attributed to the presence of defects at the counter electrode surface [43].

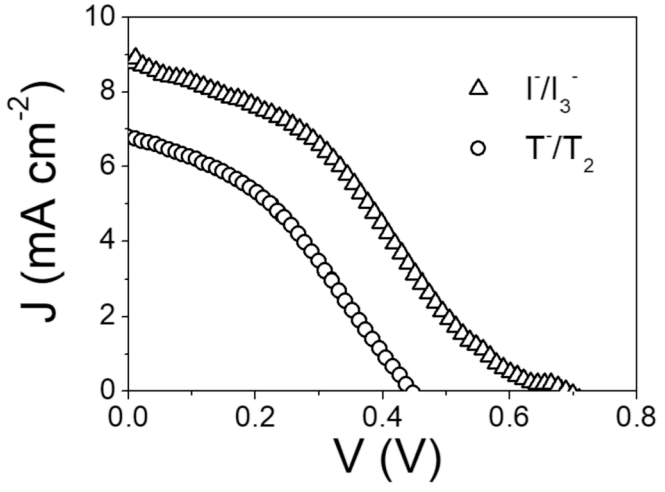

Fig. 9. *J-V* curves for DSSCs (active area = 0.25 cm^2) assembled using the rGO-QD thin film as counter electrode and liquid electrolyte containing (Δ) I^-/I_3^- or (○) T^-/T_2 redox couple, under 100 mW cm^{-2} of irradiation.

Table 2
Parameters extracted from the *J-V* curves of Fig. 7 and EIS analysis of Fig. 8, obtained for cells assembled with rGO-QD as the counter electrode and electrolytes containing different redox couples.

Electrolyte	*Jsc* (mA cm^{-2})	*Voc* (V)	*FF* (%)	*PCE* (%)	*Rs* (Ω)	*Rct* (Ω)	*CPE* (μF)
I^-/I_3^-	8.78	0.69	33	2.00	76.8	1221	53.8
T^-/T_2	7.16	0.45	35	1.14	33.8	1561	6.2

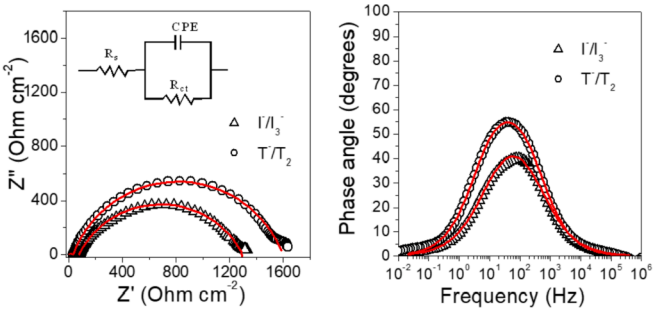

Fig. 10. (a) Nyquist and (b) Bode plots of symmetric cells of rGO-QD electrode|electrolyte|rGO-QD, filled with liquid electrolyte containing (Δ) I^-/I_3^- or (○) T^-/T_2 redox couple. The symbols represent the experimental data and the lines correspond to theoretical fitting using the R(RQ) circuit displayed on the inset.

In spite of these limitations, the DSSCs with rGO-QD counter electrode assembled here delivered reasonable responses. For comparison, cells containing a standard Pt counter electrode were prepared under the same experimental conditions, reaching a maximum *PCE* of 3.26% for the I^-/I_3^- electrolyte, and 1.14% for the T^-/T_2 electrolyte. Furthermore, cells prepared with the rGO film as counter electrode and the I^-/I_3^- electrolyte delivered a maximum *PCE* of 1.66%, indicating that the CIGSe QDs play a significant role in the reduction of the electrolyte. Thus, the DSSCs with rGO-QD counter electrode delivered a reasonable response in comparison with the standard devices assembled with the same experimental setup, thus serving as proof of concept. It is expected that cells with higher performances could be obtained by changing other parameters of the devices, such as the non-optimized TiO_2 layer (composition and thickness), as well as tuning some of the characteristics of the rGO-QD films. Some suggestions include the use of different rGO:QD ratios in the nanocomposite and the deposition of thicker films, with possibly enhanced conductivity. More importantly, it is noted that the approach discussed here might easily be transferred to the use of other types of QDs as well, which could have higher catalytic property for use in combination with I^-/I_3^- or other less corrosive redox couples.

4. Conclusion

Pyramidal shaped-like CIGSe QDs were synthesized using a microwave-assisted technique. The nanocrystals of 10 nm average size possessed a large absorption tailing and emitted light at 650 nm. The combination of these nanoparticles with GO or rGO gave composites which were processed from aqueous solutions using an automated ultrasonic spray-coating system. The optical, morphological and electrical properties of the thin films of GO-QD and rGO-QD were investigated, revealing that the presence of QDs affected significantly the characteristics of the carbonaceous materials when compared to neat films of GO and rGO. To demonstrate a possible application for the semitransparent thin films obtained, dye-sensitized solar cells were assembled using the rGO-QD film as a counter electrode and two different electrolyte compositions. The cell prepared with a commercially available I^-/I_3^--based

liquid electrolyte delivered a PCE of 2.00% and the cell prepared with a thiolate/disulfide-based electrolyte delivered a PCE of 1.14%, comparable to the value achieved with cells using a standard Pt counter electrode in the same experimental conditions. The solution processing and spray technique demonstrated here is a versatile route for the preparation of composites. This approach also shows possibilities for deposition of smooth and compact thin films on top of other types of substrates, for applications in other fields or in different types of photovoltaic technologies.

Declaration of competing interest

There is no conflict of interest.

Acknowledgements

The authors acknowledge financial support from CNPq (458413/2014-3), PIBIC/CTI and PCI/CTI, in Brazil, and the National Research Foundation (NRF), CANERGIE and Carsten trust fund, in South Africa. The authors also acknowledge LME/LNNano/CNPEM for the support in SEM analyses.

References

[1] P. Jackson, D. Hariskos, E. Lotter, S. Paetel, R. Wuerz, R. Menner, New world record eflciency for Cu(In,Ga)Se_2 thin-film solar cells beyond 20%, Prog. Photovolt. Res. Appl. 19 (2011) 894–897.

[2] I. Repins, M.A. Contreras, B. Egaas, C. DeHart, J. Scharf, C.L. Perkins, B. To, R. Noufi, 19.8%-Eflcient ZnO/CdS/CuInGaSe_2 solar cell with 81.2% fill factor, Prog. Photovolt. Res. Appl. 16 (2008) 235–239.

[3] P.-W. Li, W.-H. Zhou, Z.-L. Hou, S.-X. Wu, Synthesis of $CuIn_xGa_{1-x}Se_2$ nanocrystals for potential thin film photovoltaic application under air condition, Mater. Lett. 78 (2012) 131–134.

[4] Y.-G. Chun, K.H. Kim, K.H. Yoon, Synthesis of $CuInGaSe_2$ nanoparticles by solvothermal route, Thin Solid Films 480–481 (2005) 46–49.

[5] V.K. Kapur, M. Fischer, R. Roe, Nanoparticle oxides precursors inks for thin film copper indium gallium selenide (CIGS) solar cells, Mater. Res. Soc. 668 (2001). H2-6.

[6] S.H. Mousavi, T.S. Müller, P.W. de Oliveira, Synthesis of colloidal nanoscaled copper–indium–gallium–selenide (CIGS) particles for photovoltaic applications, J. Colloid Interface Sci. 382 (2012) 48–52.

[7] L.A. Juhaiman, L. Scoles, D. Kingston, B. Patarachao, D. Wang, F. Bensebaa, Green synthesis of tunable Cu($In_{1-x}Ga_x$)Se_2 nanoparticles using non-organic solvents, Green Chem. 12 (2010) 1248–1252.

[8] R. Seelaboyina, M. Kumar, A.V. Madiraju, K. Taneja, A.K. Keshri, S. Mahajan, K. Singh, Microwave synthesis of copper indium gallium (di)selenide nanopowders for thin film solar applications, J. Renew. Sustain. Energy 5 (2013), 031608.

[9] R. Seelaboyina, M. Kumar, A.V. Madiraju, K. Taneja, S. Kulvir, Microwave synthesis of thin film absorber layer nanopowder of copper-indium-gallium-(di) selenide and copper-zinc-tin-sulphide, Curr. Microw. Chem. 1 (2014) 6–15.

[10] I.J. Kramer, G. Moreno-Bautista, J.C. Minor, D. Kopilovic, E.H. Sargent, Colloidal quantum dot solar cells on curved and flexible substrates, Appl. Phys. Lett. 105 (2014) 163902.

[11] F. Ely, A. Matsumoto, B. Zoetebier, V.S. Peressinotto, M.K. Hirata, D.A. de Souza, R. Maciel, Handheld and automated ultrasonic spray deposition of conductive PEDOT:PSS films and their application in AC EL devices, Org. Electron. 15 (2014) 1062–1070.

[12] K.X. Steirer, M.O. Reese, B.L. Rupert, N. Kopidakis, D.C. Olson, R.T. Collins, D. S. Ginley, Ultrasonic spray deposition for production of organic solar cells, Sol. Energy Mater. Sol. Cells 93 (4) (2009) 447–453.

[13] K.D. Lee, M.J. Park, D.-Y. Kim, S.M. Kim, B. Kang, S. Kim, H. Kim, H.-S. Lee, Y. Kang, S.S. Yoon, B.H. Hong, D. Kim, Graphene quantum dot layers with energy-down-shift effect on crystalline-silicon solar cells, ACS Appl. Mater. Interfaces 7 (2015) 19043–19049.

[14] F. Soltani-kordshuli, F. Zabihi, M. Eslamian, Graphene-doped PEDOT:PSS nanocomposite thin films fabricated by conventional and substrate vibration-assisted spray coating (SVASC), Engineering Science and Technology, Int. J. 19 (2016) 1216–1223.

[15] Z. Zang, X. Zeng, M. Wang, W. Hu, C. Liu, X. Tang, Tunable photoluminescence of water-soluble AgInZnS-graphene oxide (GO) nanocomposites and their application in-vivo bioimaging, Sens. Actuators, B 252 (2017) 1179–1186.

[16] J. Wei, Z. Zang, Y. Zhang, M. Wang, J. Du, X. Tang, Enhanced performance of light-controlled conductive switching in hybrid cuprous oxide/reduced graphene oxide (Cu_2O/rGO) nanocomposites, Opt. Lett. 42 (2017) 911–914.

[17] Y.-F. Xu, M.-Z. Yang, B.-X. Chen, X.-D. Wang, H.-Y. Chen, D.-B. Kuang, C.-Y. Su, A $CsPbBr_3$ perovskite quantum dot/graphene oxide composite for photocatalytic CO_2 reduction, J. Am. Chem. Soc. 139 (2017) 5660–5663.

[18] G.G. Sonai, M.A. Melo Jr., J.H.B. Nunes, J.D. Megiatto Jr., A.F. Nogueira, Solar cells sensitized with natural dyes: an introductory experiment about solar energy for undergraduate students, Quím. Nova 38 (2015) 1357–1365.

[19] A. Kathalingam, J.-K. Rhee, S.-H. Han, Effects of graphene counter electrode and CdSe quantum dots in TiO_2 and ZnO on dye-sensitized solar cell performance, Int. J. Energy Res. 38 (2014) 674–682.

[20] L. Bai, J.N. Ding, N.Y. Yuan, H.W. Hu, Y. Li, X. Fang, Cu_2ZnSnS_4/graphene composites as low-cost counter electrode materials for dye-sensitized solar cells, Mater. Lett. 112 (2013) 219–222.

[21] J.G. Radich, R. Dwyer, P.V. Kamat, Cu_2S reduced graphene oxide composite for high-efficiency quantum dot solar cells. Overcoming the redox limitations of S_2^-/S_n^{2-} at the counter electrode, J. Phys. Chem. Lett. 2 (2011) 2453–2460.

[22] W.S. Hummers, R.E. Offeman, Preparation of graphitic oxide, J. Am. Chem. Soc. 80 (1958), 1339-1339.

[23] M. Wang, N. Chamberland, L. Breau, J.-E. Moser, R. Humphry-Baker, B. Marsan, S. M. Zakeeruddin, M. Grätzel, An organic redox electrolyte to rival triiodide/iodide in dye-sensitized solar cells, Nat. Chem. 2 (2010) 385–389.

[24] M.G. Panthani, V. Akhavan, B. Goodfellow, J.P. Schmidtke, L. Dunn, A. Dodabalapur, P.F. Barbara, B.A. Korgel, Synthesis of $CuInS_2$, and Cu(In_xGa_{1-x})Se_2 (CIGS) nanocrystal "inks" for printable photovoltaics, J. Am. Chem. Soc. 130 (2008) 16770–16777.

[25] J. Tauc, in: F. Abeles (Ed.), Optical Properties of Solids, North-Holland, Amsterdam, 1972.

[26] M. Gloeckler, J.R. Sites, Band-gap grading in Cu(In,Ga)Se_2 solar cells, J. Phys. Chem. Solids 66 (2005) 1891–1894.

[27] K. Kaviyarasu, A. Ayeshamariam, E. Manikandan, J. Kennedy, R. Ladchumananandasivam, U.U. Gomes, M. Jayachandran, M. Maaza, Solution processing of CuSe quantum dots: photocatalytic activity under RhB for UV and visible-light solar irradiation, Mater. Sci. Eng. B 210 (2016) 1–9.

[28] A. Tapley, L. Liu, X. Cui, L. Zuin, D.A. Love, J. Zhou, T.-K. Sham, Z. Ding, Assessing the band structure of $CuInS_2$ nanocrystals and their bonding with the capping ligand, J. Phys. Chem. C 119 (2015) 20967–20974.

[29] I. Ibrahim, H.N. Lim, N.M. Huang, A. Pandikumar, Cadmium sulphide-reduced graphene oxide-modified photoelectrode-based photoelectrochemical sensing platform for copper (II) ions, PLoS One 11 (2016), e0154557.

[30] M. Kamalanathan, S. Karuppusamy, R. Sivakumar, R. Gopalakrishnan, Synthesis of reduced graphene oxide-copper tin sulphide composites and their photoconductivity enhancement for photovoltaic applications, J. Mater. Sci. 50 (2015) 8029–8037.

[31] G.B. Markad, S. Battu, S. Kapoor, S.K. Haram, Interaction between quantum dots of CdTe and reduced graphene oxide: investigation through cyclic voltammetry and spectroscopy, J. Phys. Chem. C 117 (2013) 20944–20950.

[32] K.P. Mubiayi, J. Freitas, M.J. Moloto, N. Moloto, L.M. Sikhwivhilu, A.F. Nogueira, Open Phys. 14 (2016) 420–425.

[33] D. Pan, X. Wang, Z.H. Zhou, W. Chen, C. Xu, Y. Lu, Synthesis of quaternary semiconductor nanocrystals with tunable band gaps, Chem. Mater. 21 (2009) 2489–2493.

[34] K. Kaviyarasu, E. Manikandan, J. Kennedy, M. Maaza, Synthesis and analytical applications of photoluminescent carbon nanosheet by exfoliation of graphite oxide without purification, J. Mater. Sci. Mater. Electron. 27 (2016) 13080–13085.

[35] C. Punckt, M.A. Pope, J. Liu, Y. Ilhan, A. Aksay, Electrochemical performance of graphene as effected by electrode porosity and graphene functionalization, Electroanalysis 22 (2010) 2834–2841.

[36] S. Stankovich, D.A. Dikin, R.D. Piner, K.A. Kohlhaas, A. Kleinhammes, Y. Jia, Y. Wu, S.T. Nguyen, R.S. Ruoff, Synthesis of graphene-based nanosheets via chemical reduction of exfoliated graphite oxide, Carbon 45 (2007) 1558–1565.

[37] L.G. Cançado, K. Takai, T. Enoki, M. Endo, Y.A. Kim, H. Mizusaki, A. Jorio, L. N. Coelho, R. Magalhaes-Paniago, M.A. Pimenta, General equation for the determination of the crystallite size of nanographite by Raman spectroscopy, Appl. Phys. Lett. 88 (2006) 163106.

[38] A.Y.S. Eng, A. Ambrosi, C.K. Chua, F. Sanek, Z. Sofer, M. Pumera, Unusual inherent electrochemistry of graphene oxides prepared using permanganate oxidants, Chem. Eur J. 19 (2013) 12673–12683.

[39] F. Zheng, W.-L. Xu, H.-D. Jin, X.-T. Hao, K.P. Ghiggino, Charge transfer from poly (3-hexulthiophene) to graphene oxide and reduced graphene oxide, RSC Adv. 5 (2015) 89515–89520.

[40] G.B. Markad, S. Battu, S. Kapoor, S.K. Haram, Interaction between quantum dots of CdTe and reduced graphene oxide: investigation through cyclic voltammetry and spectroscopy, J. Phys. Chem. C 117 (2013) 20944–20950.

[41] G. Zhao, X. Li, M. Huang, Z. Zhen, Y. Zhong, Q. Chen, X. Zhao, Y. He, R. Hu, T. Yang, R. Zhang, C. Li, J. Kong, J.-B. Xu, R.S. Ruoff, H. Zhu, The physics and chemistry of graphene-on-surfaces, Chem. Soc. Rev. 46 (2017) 4417–4449.

[42] N. Gao, X. Fang, Synthesis and development of graphene-inorganic semiconductor nanocomposites, Chem. Rev. 115 (2015) 8294–8343.

[43] C. Nagavolu, K. Susmitha, M. Raghavender, L. Giribabu, K.B.S. Rao, C.T.G. Smith, C.A. Mills, S.R.P. Silva, V.V.S.S. Srikanth, Pt-free spray coated reduced graphene oxide counter electrodes for dye sensitized solar cells, Sol. Energy 137 (2016) 143–147.

[44] Z. Gao, L. Wang, J. Chanhg, X. Liu, D. Wu, F. Xu, Y. Guo, K. Jiang, Nitrogen doped porous graphene as counter electrode for efficient dye sensitized solar cell, Electrochim. Acta 188 (2016) 441–449.

[45] M.-H. Yeh, L.-Y. Lin, L.-Y. Chang, Y.-A. Leu, W.-Y. Cheng, J.-J. Lin, K.-C. Ho, Dye-sensitized solar cells with reduced graphene oxide as the counter electrode

prepared by a green photothermal reduction process, ChemPhysChem 15 (2014) 1175–1181.

[46] X.Y. Cheng, Z.-J. Zhou, Z.-L. Hou, W.-H. Zhou, S.-X. Wu, High performance dye-sensitized solar cell using $CuInGaSe_2$ as counter electrode prepared by sputtering, Sci, Adv. Mater. 5 (2013) 1193–1198.

[47] C.R. Dhas, A.J. Christy, R. Venkatesh, K.S. Anuratha, K. Ravichandran, A.M.E. Raj, B. Subramanian, S.K. Panda, Nebulizer spray-deposited $CuInGaS_2$ thin films, a viable candidate for counter electrode in dye-sensitized solar cells 157 (2017) 58–70.